A Robust Super-Resolution Algorithm in a Low SNR Environment for Vital Sign Radar

Sanghun YOON [1], Bong-seok KIM [2], Sangdong KIM [2,3]*

[1] Mobility Platform Research Center, Korea Electronics Technology Inst., Seongnam, Republic of Korea
[2] Division of Automotive Technology, Daegu Gyeongbuk Inst. of Science & Technology (DGIST), Daegu, Rep. of Korea
[3] Dept. of Interdisciplinary Engineering, DGIST, Daegu, Republic of Korea

shyoon11@keti.re.kr, {remnant, kimsd728}@dgist.ac.kr

Submitted February 23, 2023 / Accepted July 21, 2023 / Online first January 8, 2024

Abstract. *We propose a robust super-resolution algorithm for vital sign radar in a low signal-to-noise ratio (SNR) environment. Conventional approaches, such as fast Fourier transform and super-resolution based algorithms, suffered to provide reliable results due to the limited data length and high noise level. To overcome these limitations, our proposed algorithm utilizes a low-complexity least mean square (LMS) filter and relaxation (RELAX) techniques to achieve robust performance in low SNR environments. To evaluate the effectiveness of our algorithm, we conducted both simulation and experimental studies. Our results show that the proposed method significantly outperforms conventional methods, with Monte-Carlo simulations of respiration and heartbeat achieving an RMSE approximately 7 and 120 times lower than that of the conventional method, respectively. Overall, our algorithm provides a promising solution for robust vital sign detection in challenging low SNR environments.*

Keywords

Vital sign radar, LMS filter, RELAX, low SNR, low complexity

1. Introduction

Doppler radar has emerged as an all-round tool for a wide range of applications, including medical monitoring [1–3], vehicular sensing [4], and rescue operations. In medical settings, microwave continuous-wave (CW) Doppler radar has gained particular interest for diagnosing respiratory disorders. Several studies have focused on monitoring respiration and heartbeat during sleep to achieve high accuracy [5], with potential for sleep apnea monitoring [6]. In clinical settings, this technique has also been used as a heartbeat monitor for humans [7–9], and has recently been explored for use in radiation therapy [7]. Additionally, radar systems have been employed to monitor vital signs of animals [8], [9]. Overall, Doppler radar holds great promise as a versatile and effective tool for a range of monitoring and diagnostic applications.

Military and rescue operations require the ability to detect hidden enemies or locate victims quickly, often in challenging environments [10], [11]. In such scenarios, vital continuous-wave (CW) radar can be used to identify the location of survivors, even in disaster situations like earthquakes [12]. Additionally, due to its ability to obtain heart and respiration rates, vital signal radar has many potential applications.

However, conventional fast Fourier transform (FFT) methods for analyzing Doppler radar signals can suffer from degraded performance in low signal-to-noise ratio (SNR) environments, particularly when dealing with limited data lengths [13]. In non-contact vital radar systems, this can result in smearing and decreased accuracy and resolution. The harmonic components of respiration signals can also interfere with heartbeat signals in the Doppler spectrum environment of the FFT. Moreover, FFT analysis requires long-period windows, which may not be feasible in urgent situations, such as intensive care units, postoperative recovery, or severe trauma.

In order to address these challenges and obtain accurate frequency results, various super-resolution methods have been developed, including relaxation (RELAX), multiple signal classification (MUSIC), and estimation of signal parameters via rotational invariance techniques (ESPRIT) [14], [15]. These super-resolution algorithms represent high performance accuracy but require significant computational resources compared to the FFT-based method. However, for vital sign radar applications, a low-complexity super-resolution algorithm is needed. Considering the lower complexity of the RELAX algorithm among these methods, we choose this RELAX algorithm in this paper. Nevertheless, super-resolution algorithms that incorporate RELAX suffer from a drawback of underperforming in low SNR environments [16]. To overcome this limitation, we propose a novel approach that combines the RELAX-based super-resolution algorithm with a least mean square (LMS) filter to reduce noise power and enhance performance.

By employing our proposed algorithm, we can achieve accurate frequency results in challenging environments, including those with limited data lengths and low SNR. This

DOI: 10.13164/re.2024.0155

approach has the potential to enhance the reliability and effectiveness of vital radar systems for military and rescue operations, as well as medical applications.

The structure of this paper is consisted as follows. For the robust super-resolution algorithm in a low SNR environment for vital sign radar, Section 2 presents a basic principle of the system model. Section 3 provides the conventional ESPRIT algorithm. Section 4 shows robust super-resolution algorithm in a low SNR environment for vital sign radar. Section 5 presents the simulation and experimental results for various parameters. Section 6 represents computational complexity comparison. Finally, conclusions are shown in Sec. 7.

2. Signal Model

The transmitted signal form for the vital CW radar [17] is defined as follows:

$$s(t) = \cos\left[2\pi ft + \sigma(t)\right] \tag{1}$$

where t defines time series, f is the carrier frequency, and $\sigma(t)$ is the time-varying phase noise of the transmitted signal for CW radar. We set target's fixed distance d_0 with the time-varying displacement $x(t)$. The total distance by the body movement $d(t) = d_0 + x(t)$ and $x(t)$ can be represented by

$$x(t) = x_{\mathrm{h}}(t) + x_{\mathrm{r}}(t) \approx a_{\mathrm{h}} \sin(\omega_{\mathrm{h}} t) + a_{\mathrm{r}} \sin(\omega_{\mathrm{r}} t) \tag{2}$$

where $x_{\mathrm{h}}(t)$ and $x_{\mathrm{r}}(t)$ denote the body movements of the heartbeat and the respiration signal, respectively. The movement signal can be represented with amplitude a_{h} and a_{r} and angular frequency ω_{h} and ω_{r}, respectively.

The received signal $y(t)$, which is reflected from the human body, can be represented as

$$y(t) \approx \cos\left[2\pi ft - \frac{4\pi}{\lambda}\left(d_0 - x(t)\right) + \sigma\left(t - \frac{2d_0}{C}\right)\right] + \psi(t) \tag{3}$$

where C denotes the propagation speed, $\lambda = C/f$ is the wavelength, and $\psi(t)$ is the additive white Gaussian noise (AWGN) signal. After $y(t)$ is converting into the baseband signal [16], the down-sampling signals $p(t)$ consists of the respiration harmonics due to the nonlinear phase modulation and heartbeat movement as

$$p(t) = \exp\left[\frac{\mathrm{j}4\pi}{\lambda}\left(x_{\mathrm{h}}(t) + \sum_{m=1}^{M} x_{\mathrm{r},m}(t) + \theta\right)\right] + \psi(t) \tag{4}$$

where $x_{\mathrm{r},m}(t)$ means the m-th harmonic component of respiration with amplitude $a_{\mathrm{r},m}$ and angular frequency $\omega_{\mathrm{r},m}$ for $m = 1, 2, \ldots, M$. For example, the original respiration component is defined as $m = 1$ and θ represents the total accumulated phase residual. After sampling with a sampling frequency of $f_{\mathrm{s}} = 1/T_{\mathrm{s}}$, the phase value $q[n]$ of the discrete time model $p[n]$ for $n = 0, 1, \ldots, N–1$ can be expressed such as

$$\begin{aligned} d[n] &= \tan^{-1}\left(\frac{\mathrm{Im}(p[n])}{\mathrm{Re}(p[n])}\right) \\ &= \frac{4\pi x_{\mathrm{h}}[n]}{\lambda} + \frac{4\pi}{\lambda}\sum_{m=1}^{M} x_{\mathrm{r},m}[n] + \theta + \zeta[n] \end{aligned} \tag{5}$$

where $\mathrm{Re}(\cdot)$ and $\mathrm{Im}(\cdot)$ are the real value and imagery value, respectively and $\zeta[n]$ is the arctangent result of the AWGN noise.

3. Conventional ESPRIT Algorithm

The existing ESPRIT algorithm is widely used to obtain the super-resolution results. Through the received signal $d[k]$, the autocorrelation matrix $\mathbf{R}_{dd}$ is expressed such as

$$\mathbf{R}_{dd} = \sum_{m=0}^{N-L} \mathbf{d}\mathbf{d}^{\mathrm{H}} \tag{6}$$

where the received sequence defines $\mathbf{d} = [d[m], \ldots, d[m + L - 1]]^{\mathrm{T}}$, L means the parameter of selection for $2 \le L < N$, and $(\cdot)^{\mathrm{H}}$ is the Hermitian transpose. The forward-backward autocorrelation $\mathbf{R}_{\mathrm{fb}}$ is calculated as:

$$\mathbf{R}_{\mathrm{fb}} = \frac{1}{2}(\mathbf{R}_{dd} + \mathbf{J}\mathbf{R}^{*}_{dd}\mathbf{J}) \tag{7}$$

where $\mathbf{J}$ is the exchange matrix of L by L.

The forward-backward autocorrelation $\mathbf{R}_{\mathrm{fb}}$ can be resolved through the eigenvalue decomposition (EVD) by

$$\mathbf{R}_{\mathrm{fb}} = \begin{bmatrix}\mathbf{S} & \mathbf{N}\end{bmatrix}\begin{bmatrix}\lambda_0 & 0 & \vdots & 0 \\ 0 & \lambda_1 & \ddots & \vdots \\ \vdots & \ddots & \ddots & 0 \\ 0 & \cdots & 0 & \lambda_{L-1}\end{bmatrix}\begin{bmatrix}\mathbf{S}^{*} \\ \mathbf{N}^{*}\end{bmatrix} \tag{8}$$

where the signal eigenvector matrix $\mathbf{S} = [\mathbf{s}_0, \ldots, \mathbf{s}_M]$ consists of $M + 1$ eigenvectors which span the signal subspace of the correlation matrix, the noise eigenvector matrix $\mathbf{N} = [\mathbf{n}_0, \ldots, \mathbf{n}_{L-M-2}]$ means $L - M - 1$ eigenvectors which span the noise subspace of the correlation matrix, and λ_n denotes the n-th eigenvalues of $\mathbf{R}_{\mathrm{fb}}$. And, $M + 1$ means the total number of the respiration and heart frequency. The largest $M + 1$ eigenvalues of $\lambda_0, \ldots, \lambda_M$ correspond to the $M + 1$ eigenvectors of $\mathbf{S}$. The other eigenvalues $\lambda_{M+1}, \ldots, \lambda_{L-1}$ correspond to the eigenvectors of $\mathbf{N}$ such that $\lambda_{M+1} = \ldots = \lambda_{L-1} = \sigma^2$. We can present the $\mathbf{S}_1$ and $\mathbf{S}_2$ matrices, getting rid of the last row vector and the first row vector, respectively, such that $\mathbf{S}_1 = [\mathbf{I}_{L-1} \ \ \mathbf{0}_{1\times(L-1)}]\mathbf{S}$, $\mathbf{S}_2 = [\mathbf{0}_{1\times(L-1)} \ \ \mathbf{I}_{L-1}]\mathbf{S}$, $\mathbf{I}_M$ denotes an identity matrix of M by M, and $\mathbf{0}_{M\times N}$ is a zero matrix of M by N. Sub-matrices $\mathbf{S}_1$, $\mathbf{S}_2$ are resolved by

$$\mathbf{S}_1 = [\mathbf{I}_{L-1}\mathbf{0}_{1\times(L-1)}]\mathbf{A}\mathbf{T}, \ \mathbf{S}_2 = [\mathbf{I}_{L-1}\mathbf{0}_{1\times(L-1)}]\mathbf{A}\mathbf{\Phi}\mathbf{T} \tag{9}$$

where $\mathbf{A} = [\mathbf{a}(\omega_{\mathrm{r},0}) \ \mathbf{a}(\omega_{\mathrm{r},1}) \ \ldots \ \mathbf{a}(\omega_{\mathrm{r},M-1}) \ \mathbf{a}(\omega_{\mathrm{h}})]$, $\mathbf{a}(\omega_{\mathrm{r},m}) = [1, \exp(-\mathrm{j}\omega_{\mathrm{r},m}), \ldots, \exp(-\mathrm{j}(L-1)\omega_{\mathrm{r},m})]^{\mathrm{T}}$, $\mathbf{a}(\omega_{\mathrm{h}}) = [1 \ \exp(-\mathrm{j}\omega_{\mathrm{h}})$,

…, $\exp(-\mathrm{j}(L-1)\omega_\mathrm{h})]^\mathrm{T}$, $\mathbf{\Phi} = \mathrm{diag}[\exp(-\mathrm{j}\omega_{\mathrm{r},0}), \exp(-\mathrm{j}\omega_{\mathrm{r},1}),\ldots, \exp(-\mathrm{j}\omega_{\mathrm{r},M-1}), \exp(-\mathrm{j}\omega_\mathrm{h})]$ and $\mathbf{T}$ denotes the non-singular transformation matrix of $M+1$ by $M+1$. The sub-matrices are performed by a pseudo inverse such as

$$\mathbf{C} = \mathbf{S}_1^{\dagger}\mathbf{S}_2 \tag{10}$$

where $\mathbf{C} = \mathbf{T}^{-1}\mathbf{\Phi}\mathbf{T}$ and † denotes the Moore-Penrose pseudo inverse. We can then acquire the heartbeat frequency f_h with the last element of $\mathbf{\Phi}$ and the eigenvalues of $\mathbf{C}$ such as

$$\hat{f}_\mathrm{h} = \frac{1}{2\pi}\angle(\exp(\mathrm{j}\omega_\mathrm{h})) \tag{11}$$

where $\angle(\cdot)$ means the phase angles for a complex signal. However, this conventional ESPRIT algorithm costs high computational load, so that we propose a super-resolution algorithm of the low complexity.

4. Robust Super-Resolution Algorithm in a Low SNR Environment for Vital Sign Radar

The proposed algorithm consists of three stages: classification of respiration and heartbeat signals, SNR improvement, and Doppler estimation by RELAX.

In the classification stage, the received signal is differentiated into a respiration signal and a heartbeat signal by respiration low-pass filtering (LPF) and heartbeat high-pass filtering (HPF), respectively. And then the LMS filter is applied to each signal as shown in Fig. 1. The respiration signal power is so prominent that the heartbeat signal is buried under it. Accordingly, to acquire the heartbeat signal, sharp fixed respiration LPF and heartbeat HPF are applied to the received signal. The cut-off parameters of a sharp respiration LPF and the heartbeat HPF are based on the statistics of the heartbeat in [20]. With the received signal vector $\mathbf{d} = [d[0], d[1],\ldots, d[N-1]]$, the respiration low-pass filtered output $d_\mathrm{L}[n]$ can be accomplished using the parameters of the passband frequency at 0.4 Hz (24 beats/min) and the stopband frequency at 0.6 Hz (36 beats/min), and the heartbeat high-pass filtered output $d_\mathrm{H}[n]$ with a stopband frequency of 0.7 Hz (42 beats/min) and a passband frequency of 0.8 Hz (48 beats/min) can be achieved, respectively.

The proposed pre-processing method for the SNR improvement is shown. From (5), to clarify the received signal model, the following explanation removes the noise term, $\zeta[n]$, for simplicity. In the SNR improvement stage, noise cancellation using the LMS algorithm [18] assumes a respiration FIR filter with adjustable coefficients, $h_\mathrm{r}[k]$, $k = 0,1,\ldots,K-1$, such as

$$s_\mathrm{r}[n] = \sum_{k=0}^{K-1} h_\mathrm{r}[k]\cdot d_\mathrm{L}[n-D-k], \quad n = 0,\ldots,N-1 \tag{12}$$

where $s_\mathrm{r}[n]$ is the result of the adaptive respiration filter, and D is the decorrelation parameter ($D \geq 1$). The error signal, which optimizes the respiration FIR filter, is given by $e_\mathrm{r}[n] = d_\mathrm{L}[n] - \hat{s}_\mathrm{r}[n]$, where $\hat{s}_\mathrm{r}[n]$ is used to estimate $d_\mathrm{L}[n]$. Equation (13) is obtained by the LMS algorithm, which provides an alternative computational method for determining the optimum filter coefficients $h_\mathrm{r}[k]$. The LMS algorithm is basically a recursive gradient (steepest-descent) method that finds the minimum error and thus achieves the set of optimum filter coefficients. The minimization of the squared error yields the optimum coefficient $h_\mathrm{r}[k]$, which is used by the characteristic function such as

$$h_{\mathrm{r},n}[k] = h_{\mathrm{r},n-1}[k] + \beta_\mathrm{r} e_\mathrm{r}[n] d_\mathrm{L}[n-D-k] \tag{13}$$

where $h_{\mathrm{r},n}[k]$ denotes the n-th filter coefficients, and β_r is the step size, which controls convergence of the adaptation process for the respiration signal. The LMS filter of the heartbeat signal is the same as that of the respiration signal with the results of the adaptive heartbeat filter $s_\mathrm{h}[n]$.

The vital Doppler spectrum as the RELAX results need to determine the order of the process p which is equal to the number of targets M. In case of the order $p > M$, the results of the vital Doppler spectrum will be smoothed and will have low resolution. When the order p is larger than M, the results of the spectrum will have spurious peaks. The method of determining the model order p is consisted of the Akaike information criterion (AIC) and minimum description length (MDL) [22], [22]. The optimal modeling order can be selected by changing the model order until the values of the MDL or the AIC are minimized.

After the number of order p, we can achieve the RELAX algorithm to enhance the vital Doppler resolution. The filtered respiration signal $\mathbf{S}_\mathrm{r} = [s_\mathrm{r}[0], s_\mathrm{r}[1],\ldots, s_\mathrm{r}[N-1]]$ is fed into the input of the RELAX algorithm in order to estimate the respiration frequency accurately. The heartbeat signal is also obtained through the RELAX. After this process, we repeat first step for $m = 1, 2,\ldots, M$ in order to obtain the estimated respiration frequency and amplitude of the m-th harmonic. The m-th estimated respiration frequency $\hat{f}_{\mathrm{r},m}$ is calculated as follows:

$$\hat{f}_{\mathrm{r},m} = \arg\max_{f_\mathrm{r}} \frac{\left\|\boldsymbol{\alpha}^\mathrm{H}(f_\mathrm{r})\mathbf{S}_\mathrm{r}\right\|^2}{\left\|\boldsymbol{\alpha}(f_\mathrm{r})\right\|^2} \tag{14}$$

where $\boldsymbol{\alpha}(f_\mathrm{r}) = [1, \exp(\omega_\mathrm{r}),\ldots, \exp(\omega_\mathrm{r}(N-1))]^\mathrm{T}$ and the m-th estimated amplitude $\hat{a}_m$ is as obtained as follows:

$$\hat{a}_{\mathrm{r},m} = \frac{\boldsymbol{\alpha}^\mathrm{H}(\hat{f}_{\mathrm{r},m})\mathbf{S}_\mathrm{r}}{\left\|\boldsymbol{\alpha}(\hat{f}_{\mathrm{r},m})\right\|^2}. \tag{15}$$

The respiration RELAX algorithm finishes when the maximum value of $\|\boldsymbol{\alpha}^\mathrm{H}(f_\mathrm{r})\mathbf{S}_\mathrm{r}\|^2$ results is less than a pre-determined threshold. The heartbeat RELAX is achieved as the respiration RELAX procedure.

The proposed structure can be summarized according to the flowchart depicted in Fig. 2. Initially, the algorithm receives the input signal. Following that, it employs low-pass

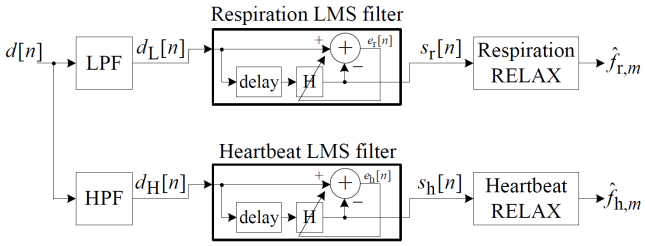

Fig. 1. Block diagram of the Doppler spectrum estimator using the proposed algorithm.

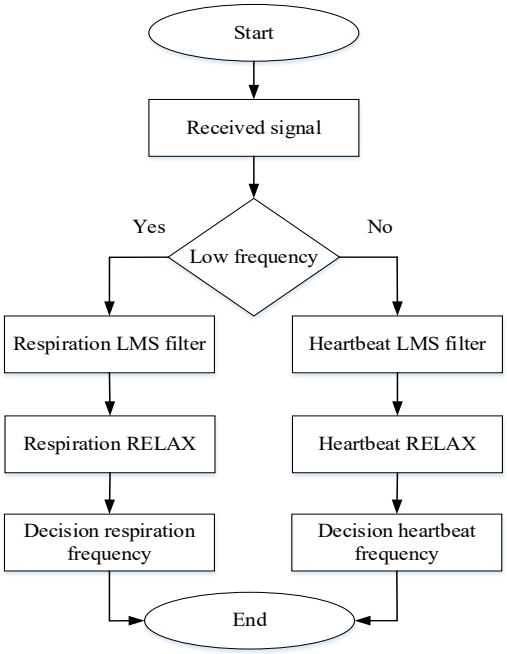

Fig. 2. Flowchart of the proposed structure.

filtering (LPF) and high-pass filtering (HPF) to determine whether the received signal corresponds to a low-frequency signal, effectively distinguishing between the respiration and heartbeat signals. Subsequently, separate LMS filters are applied to the extracted respiration and heartbeat signals. Finally, the signals that have passed through their respective LMS filters perform accurate frequency estimation of the respiration and heartbeat signals using the RELAX algorithm. These steps contain the entire process.

5. Simulation and Experimental Results

To evaluate the effectiveness of our proposed algorithm, we conducted a Monte-Carlo simulation and obtained results for the Doppler spectrum. We performed 10,000 estimates to ensure statistical significance. In the simulation, we used a harmonic model of vital signs to generate signals for respiration and heartbeat, with frequencies of 0.3 Hz (18 beats/min) and 1.05 Hz (63 beats/min), respectively. The respiration signal was modeled using 5 harmonics, with amplitudes satisfying the following: $a_{r1} : a_{r2} : a_{r3} : a_{r4} : a_{r5} : a_h = 10 : 4 : 0.1 : 0.02 : 0.05 : 2$. We compared the results of the FFT, the conventional ESPRIT, the conventional MUSIC, and the proposed algorithm to detect the vital signs. The reflected signal was sampled at 20 Hz. To clarify the performance differences due to SNR, the SNR values of simulation were set to 3 dB and 50 dB, respectively.

Figure 3 illustrates the Doppler spectrum results obtained from the FFT, ESPRIT, MUSIC, and the proposed method. In Fig. 3(a), which represents a challenging SNR environment of 3 dB, the heartbeat signal estimation by conventional ESPRIT, MUSIC, and FFT algorithms was not

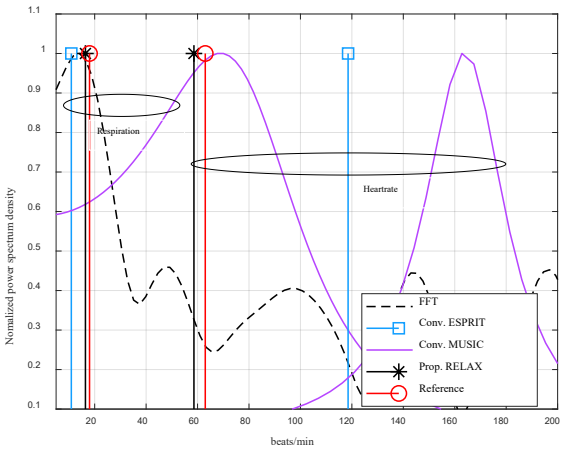

(a)

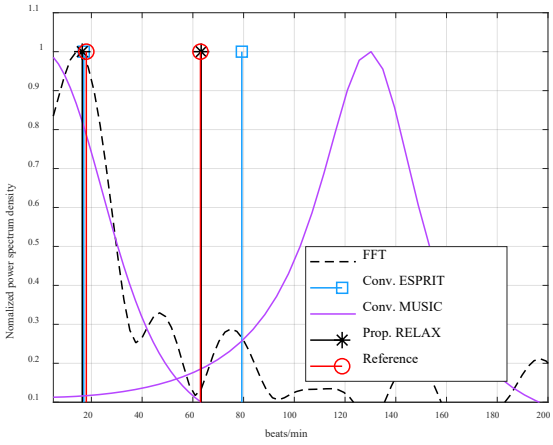

(b)

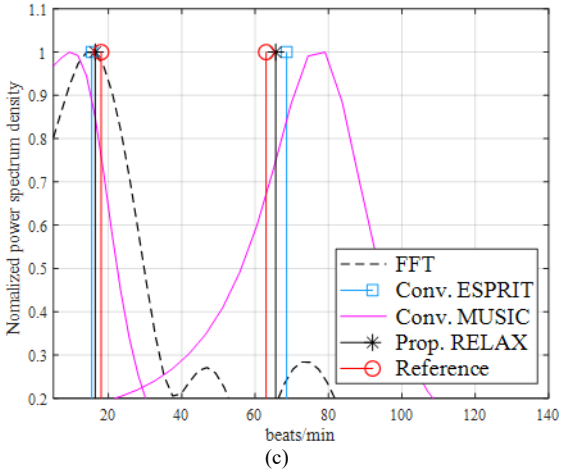

(c)

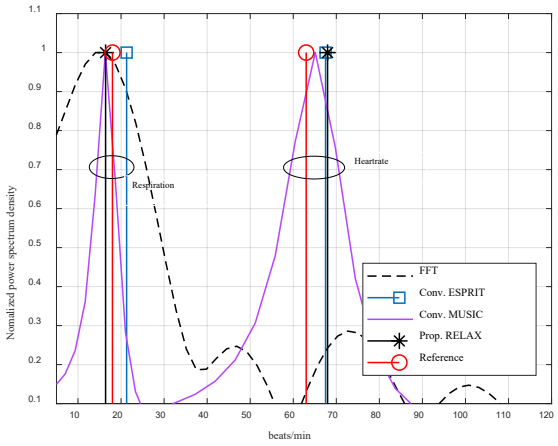

(d)

Fig. 3. Doppler spectrum of various algorithms at SNR: (a) 3 dB, (b) 10 dB, (c) 20 dB, and (d) 50 dB.

accurate. In contrast, the results of the proposed algorithm demonstrated similar to the beats per minute of reference for heartbeat. As depicted in Fig. 3(b) with an SNR of 10 dB, the accuracy of conventional algorithms improved as the noise decreased, but only the proposed method maintained good performance. Similarly, in Fig. 3(c), where the noise was further reduced compared to Fig. 3(b), conventional algorithms represent improved accuracy. Figure 3(d) shows the scenario with an SNR of 50 dB, showing that all algorithms yielded results similar to the reference. The results from Fig. 3 indicate that when the SNR is high, all algorithms perform well, but in low SNR conditions, only the proposed method enhances performance.

These results demonstrate that while all algorithms operate effectively in high SNR environments, only the proposed algorithm maintains its efficacy in low SNR conditions. This implies that even in real radar applications with low SNR environments, the proposed algorithm remains functional. Notably, for heartbeat signals, where the SNR is low due to signal propagation through the chest, the proposed algorithm demonstrates superior performance despite the challenging conditions.

In Fig. 4, the root mean square error (RMSE) according to the SNR of each algorithm was calculated with C times for heartbeat Doppler signals with a short duration. The RMSE is defined by $\sqrt{1/C \sum_{m=1}^{C} (\hat{f}_m - f)^2}$, where C is set to 10,000 and $\hat{f}_m$ is the estimated frequency of the respiration or heartbeat in the m-th Monte-Carlo trial, respectively.

By analyzing the data presented in Fig. 4, we simulated the root mean square error (RMSE) for each algorithm based on the parameter differences in the estimation of respiration and heartbeat signals, which are vital Doppler signals. Figure 4(a) displays the results for the respiration estimation of the detected target when varying the SNR from –10 to 20 dB. The reference frequency for comparison is set at 0.3 Hz (18 beats per minute) for respiration. In terms of SNR, the proposed algorithm outperforms other methods such as MUSIC, with the ESPRIT algorithm representing the poorest performance for respiration signal estimation.

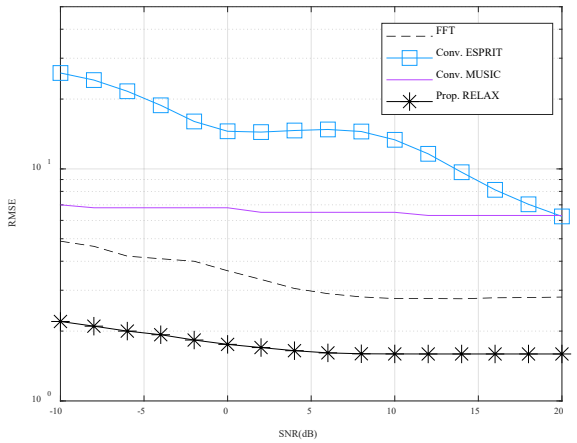

(a)

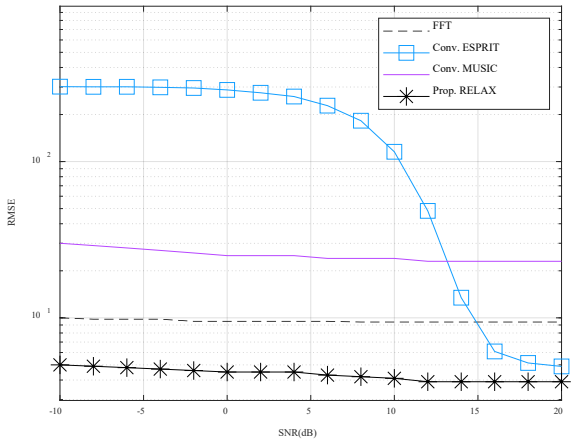

(b)

Fig. 4. RMSEs of (a) the respiration and (b) the heartbeat signals.

Notably, for an SNR of 10 dB, the RMSE of the proposed algorithm is approximately 7 times lower than that of the conventional ESPRIT algorithm in Fig. 4(a).

Moreover, in Fig. 4(b), which focuses on heartbeat parameters, the proposed algorithm demonstrates superior performance compared to conventional FFT, ESPRIT, and MUSIC algorithms. The RMSE of the proposed algorithm is approximately 120 times lower than that of the conventional ESPRIT algorithm for heartbeat signal estimation.

Overall, the results indicate that the proposed algorithm exhibits significantly improved accuracy compared to conventional methods for both respiration and heartbeat signal estimation, showing its superior performance in terms of RMSE.

To validate the efficacy of the proposed method in a real environment, we conducted experiments using the iMotion radar [17], [19] at Texas Tech University. For these experiments, we employed a 2.4 GHz continuous wave (CW) RF module consisting of one transmitted channel and one received channel. The transmitted output power was set to –3 dBm. The receiver component comprised several elements, including a low noise amplifier (LNA), a bandpass filter (BPF), a gain block, a mixer, and a baseband operational amplifier (OP). The LNA amplified the 2.4 GHz signal with a gain of 19 dB. The signal, after being filtered by

the BPF, was then amplified by a gain block with a gain of 12.3 dB and an input-referred P1dB of 1 dBm. The mixer down-converted the signal directly to baseband. The resulting signals from the mixer were further amplified by the baseband OP with a voltage gain of 40 dB.

From the human body, a CW radar signal $s(t)$ is returned back. After this reflected signal was down-converted, the zero-IF signals $p(t)$ can be used for the analysis of the vital sign data. In an indoor room, we made experiments to verify the proposed method for a vital sign. The parameter of experiment followed the parameters of the simulation. When the target was located at R = 0.2 m, the Doppler spectrum of the heartbeat rate was obtained, as shown in Fig. 5 and Fig. 6. We focused on the heartbeat signal in experiments because the heartbeat is sensitive with a low SNR. As seen in Fig. 5 and Fig. 6, the proposed method estimated the peak of the heartbeat frequency well compared with the reference [20] while the conventional ESPRIT, MUSIC, and FFT methods could not estimate it accurately relative to the exact heartbeat frequency at one randomly chosen frame.

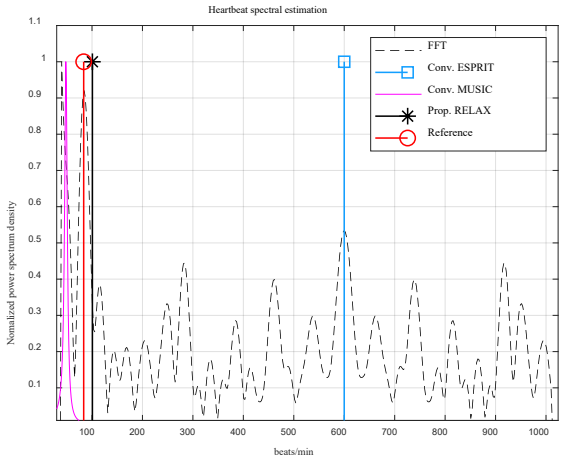

Fig. 5. One randomly chosen frame: the experimental results from iMotion radar in the case of the heartbeat signal.

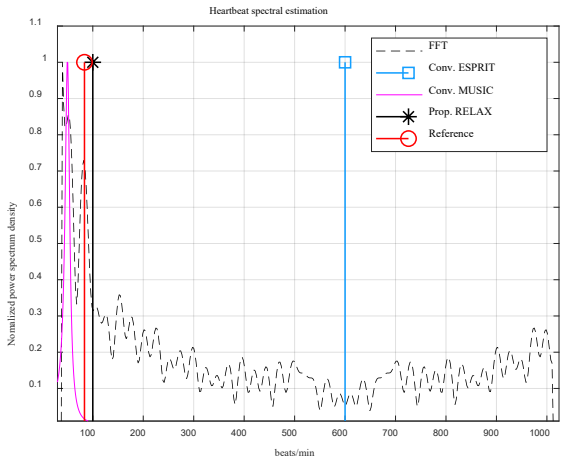

Fig. 6. Second randomly chosen frame: the experimental results from iMotion radar in the case of the heartbeat signal.

6. Computational Complexity Comparison

To evaluate the efficiency of our proposed algorithm in terms of processing time, we implemented and compared various methods using MATLAB. We used the CPUTIME function in MATLAB to measure the computational burden of the algorithms. The conventional ESPRIT algorithm involves matrix computations, which require eigenvalue decomposition and matrix inversions in MATLAB. In contrast, our proposed RELAX algorithm has less complexity because it consists of a combination of FFT algorithms. We applied the FMCW chirp parameters used in the previous Monte-Carlo simulations to assess the computational complexity of the algorithms. Figure 7 shows a comparison of the total processing time required for the conventional ESPRIT algorithm and our proposed algorithm. As shown in Fig. 7(a) and (b) for respiration and heartbeat respectively, the proposed algorithm has much lower complexity due to the use of low complexity FFT algorithms.

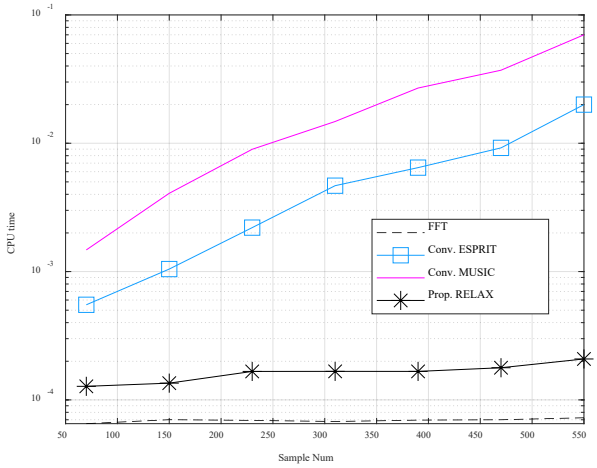

(a)

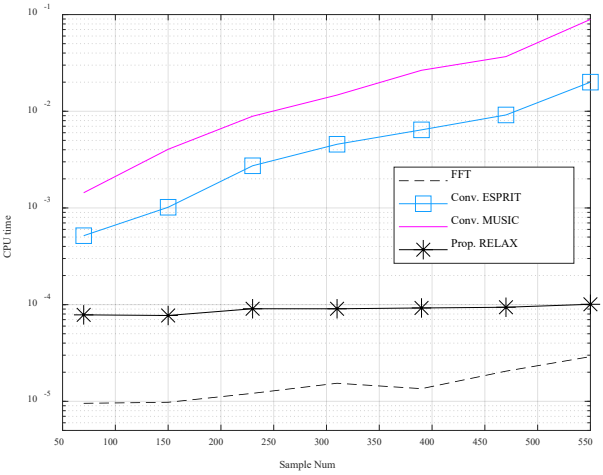

(b)

Fig. 7. MATLAB CPU execution time of algorithms for: (a) respiration and (b) heartbeat.

7. Conclusions

We proposed a robust super-resolution algorithm for vital sign radar to accurately estimate the heart and respiration rates of the human body in a low SNR environment. Super-resolution algorithms are essential in vital sign radar, but they often suffer from poor performance in low SNR environments and high computational complexity. To address these problems, our proposed algorithm combines a LMS filter and RELAX algorithm, which cancels interference signals successively to achieve high resolution. The algorithm uses the EVD operation to distinguish signal and noise components, but in a low SNR environment, it is difficult to successfully distinguish between them due to high noise levels. Monte-Carlo simulation results show that our proposed method outperforms conventional ESPRIT and MUSIC methods in terms of root mean square error (RMSE). Specifically, for respiration signals with a SNR of 10 dB, the RMSE of our proposed method is about 7 times lower than that of the conventional ESPRIT method. For heartbeat signals, the RMSE of our proposed algorithm is about 120 times lower than that of the conventional algorithm. To compare the processing time of our proposed algorithm with conventional ESPRIT and MUSIC, we designed and implemented various methods using MATLAB. The results show that our proposed algorithm has much less complexity than conventional ESPRIT and MUSIC because it is composed of low complexity FFT algorithms. By combining the LMS filter and RELAX algorithm, our proposed algorithm provides a robust and efficient solution for vital sign radar applications in low SNR environments. Our future research aims to focus on advancing the field of vital sign radar by developing imaging capabilities that can simultaneously extract distance and angle information. This will be accomplished through the utilization of super-resolution techniques. By incorporating these techniques into vital sign radar, we intend to enhance the accuracy and precision of vital sign measurements, thereby enabling more comprehensive and detailed radar imaging.

Acknowledgments

This work was supported by the DGIST R&D Program of the Ministry of Science and ICT, Korea (24-IT-01), by the Basic Science Research Program through the National Research Foundation of Korea (NRF) funded by the Ministry of Education (2022R1F1A1063386) and by the Institute of Information & Communications Technology Planning & Evaluation (IITP) grant funded by the Korea government (MSIT) (No. 2022-0-00521, Development of 5G-NR-V2X communication technology to support over Lv.4 autonomous driving service).

References

[1] KIM, S., KIM, B., JIN, Y., et al. Extrapolation-RELAX estimator based on spectrum partitioning for DOA estimation of FMCW radar. *IEEE Access*, 2019, vol. 7, p. 98771–98780. DOI: 10.1109/ACCESS.2019.2930102

[2] WU, Q., MEI, Z., LAI, Z., et al. A non-contact vital signs detection in a multi-channel 77GHz LFMCW radar system. *IEEE Access*, 2021, vol. 9, p. 49614–49628. DOI: 10.1109/ACCESS.2021.3068480

[3] XIA, W., LI, Y., DONG, S. Radar-based high-accuracy cardiac activity sensing. *IEEE Transactions on Instrumentation and Measurement*, 2021, vol. 70, p. 1–13. DOI: 10.1109/TIM.2021.3050827

[4] KHAN, F., AZOU, S., YOUSSEF, R., et al. IR-UWB radar-based robust heart rate detection using a deep learning technique intended for vehicular applications. *Electronics*, 2022, vol. 11, p. 1–15. DOI: 10.3390/electronics11162505

[5] KWON, H., CHOI, S., LEE, D., et al. Attention-based LSTM for non-contact sleep stage classification using IR-UWB radar. *IEEE Journal of Biomedical and Health Informatics*, 2021, vol. 25, no. 10, p. 3844–3853. DOI: 10.1109/JBHI.2021.3072644

[6] KWON, H., SON, D., LEE, D., et al. Hybrid CNN-LSTM network for real-time apnea-hypopnea event detection based on IR-UWB radar. *IEEE Access*, 2022, vol. 10, p. 17556–17564. DOI: 10.1109/ACCESS.2021.3081747

[7] FALLATAH, A., BOLIC, M., MACPHERSON, M., et al. Monitoring respiratory motion during VMAT treatment delivery using ultra-wideband radar. *Sensors*, 2022, vol. 22, no. 6, p. 1–16. DOI: 10.3390/s22062287

[8] MA, Y., WANG, P., XUE, H., et al. Non-contact vital states identification of trapped living bodies using ultra-wideband bio-radar. *IEEE Access*, 2021, vol. 9, p. 6550–6559. DOI: 10.1109/ACCESS.2020.3048381

[9] TANG, D., RODRIGUES, D. V. Q., BROWN, M. C., et al. Dual null detection points removal and time-domain sensitivity analysis of a self-injection-locked radar for small-amplitude motion sensing. *IEEE Transactions on Microwave Theory and Techniques*, 2022, vol. 70, no. 9, p. 4263–4272. DOI: 10.1109/TMTT.2022.3186299

[10] LI, Z., JIN, T., LI, L., et al. Spatiotemporal processing for remote sensing of trapped victims using 4-D imaging radar. *IEEE Transactions on Geoscience and Remote Sensing*, 2023, vol. 61, p. 1–12. DOI: 10.1109/TGRS.2023.3266039

[11] DOGRU, S., MARQUES, L. Through-wall mapping using radar: Approaches to handle multipath reflections. *IEEE Sensors Journal*, 2021, vol. 21, no. 10, p. 11674–11683. DOI: 10.1109/JSEN.2021.3067721

[12] PHAM, L., PAUL, M., PRASAD, P. Noncontact detection of cardiopulmonary activities of trapped humans in rescue relief events. *IEEE Access*, 2022, vol. 10, p. 75680–75692. DOI: 10.1109/ACCESS.2022.3190902

[13] WANG, Y., SHUI, Y., YANG, X., et al. Multi-target vital signs detection using frequency-modulated continuous wave radar. *EURASIP Journal on Advances in Signal Processing*, 2021, p. 1 to 19. DOI: 10.1186/s13634-021-00812-9

[14] LIN, Y., LEE, T. Max-MUSIC: A low-complexity high-resolution direction finding method for sparse MIMO radars. *IEEE Sensors Journal*, 2020, vol. 20, no. 24, p. 14914–14923. DOI: 10.1109/JSEN.2020.3009426

[15] HU, Y., DENG, W., ZHANG, X., et al. FDA-MIMO radar with long-baseline transmit array using ESPRIT. *IEEE Signal Processing Letters*, 2021, vol. 28, p. 1530–1534. DOI: 10.1109/LSP.2021.3095612

[16] SUN, R., ZHANG, W., YAO, B. Frame arrival detection for low SNR frequency selective fading channels. In *2018 IEEE/CIC International Conference on Communications in China (ICCC)*. Beijing (China), 2018, p. 374–378. DOI: 10.1109/ICCChina.2018.8641184

[17] LI, C., LIN, J. Random body movement cancellation in Doppler

radar vital sign detection. *IEEE Transactions on Microwave Theory and Techniques*, 2008, vol. 56, no. 12, p. 3143–3152. DOI: 10.1109/TMTT.2008.2007139

[18] ARDALAN, S., MOGHADAMI, S., JAAFARI, S. Motion noise cancelation in heartbeat sensing using accelerometer and adaptive filter. *IEEE Embedded Systems Letters*, 2015, vol. 7, no. 4, p. 101 to 104. DOI: 10.1109/LES.2015.2457933

[19] LI, Y., GU, C., NIKOUBIN, T., et al. Wireless radar devices for smart human-computer interaction. In *IEEE 57th International Midwest Symposium on Circuits and Systems (MWSCAS)*. College Station (TX, USA), 2014, p. 65–68. DOI: 10.1109/MWSCAS.2014.6908353

[20] TOTH-LAUFER, E., VARKONYI-KOCZY, A. Personal-statistics-based heart rate evaluation in anytime risk calculation model. *IEEE Transactions on Instrumentation and Measurement*, 2015, vol. 64, no. 8, p. 2127–2135. DOI: 10.1109/TIM.2014.2376111

[21] AKAIKE, H. Fitting autoregressive models for prediction. *Annals of the Institute of Statistical Mathematics*, 1969, vol. 21, p. 243–247. DOI: 10.1007/BF02532251

[22] RISSANEN, J. Modeling by shortest data description. *Automatica*, 1978, vol. 14, p. 465–471. DOI: 10.1016/0005-1098(78)90005-5

About the Authors …

Sanghun YOON was born in Seoul, South Korea, in 1973. He received the B.S., M.S. and Ph.D. degrees in Electronics Engineering from Hanyang University, Seoul, Korea, in 1996, 1998, and 2008 respectively. From 2009 to 2012, he was a senior researcher of Sensor Interface Research Team in Electronics and Telecommunications Research Institute (ETRI). Currently, he is working at SoC Platform Research Center in Korea Electronics Technology Institute (KETI) as a senior researcher. His current research interests include wireless communication system, V2X communication systems such as WAVE, wireless localization system, and SoC design & system verification.

Bong-seok KIM was born in Daegu, South Korea, in 1978. He received his B.S. degree in Electronics Engineering in 2006 as well as his M.S. and Ph.D. degrees in Information and Communications Engineering from Yeungnam University, Korea in 2009 and 2014, respectively. Since 2014, he has worked at the DGIST, Korea as a senior research engineer. His current interests include multi-functional radar systems and radar signal processing.

Sangdong KIM (corresponding author) was born in Seoul, South Korea, in 1981. He received the B.S. degree from Hanyang University, in 2004, the M.S. degree from Hanyang University, in 2006, and the Ph.D. degree from Kyungpook National University, in 2018, all in Electronics Engineering. From 2015 to 2016, he was a Visiting Scholar with the University of Florida. Since 2006, he has been a Principal Researcher with the Division of Automotive Technology at the DGIST. Since 2020, he has also worked as an Associate Professor (Adj.) with the Interdisciplinary Engineering at the DGIST. Since 2022, he is a Visiting Scholar with the Pennsylvania State University. His research interests include super-resolution algorithms, automotive radar, vital radar, and deep learning-based radar.